Supplementary information

Phosphine-Induced Conversion from Au_{36} to Au_{32} for Constructing High-Performance CO_2RR Catalyst

Jiansheng Ye,[a] Yali Dai,[a] Wenjun Liu,[b] Jingrou Xu,[a] Jialing Li,[a] Meng Chen,[c] Sha Yang,[b] Qinzhen Li,*[a] Yuanxin Du,*[a] Jinsong Chai,*[a] and Manzhou Zhu

[a]Department of Materials Science and Engineering, Anhui University, Hefei, Anhui 230601,China.

[b]Department of Chemistry and Centre for Atomic Engineering of Advanced Materials, Key Laboratory of Structure and Functional Regulation of Hybrid Materials of Ministry of Education, Institutes of Physical Science and Information Technology and Anhui Province Key Laboratory of Chemistry for Inorganic/Organic Hybrid Functionalized Materials, Anhui University, Hefei, Anhui 230601, China.

[c]Jingdezhen University, Jingdezhen, Jiangxi 333000, China.

* Corresponding author. qinzhenlee@163.com; duyuanxin@ahu.edu.cn; chaijs@ahu.edu.cn

Table S1 The Au_{36} ratio of Au and S in SC-XRD and XPS.

Test project	Au	S
SC-XRD[1]	36	24
XPS	36.00	24.03

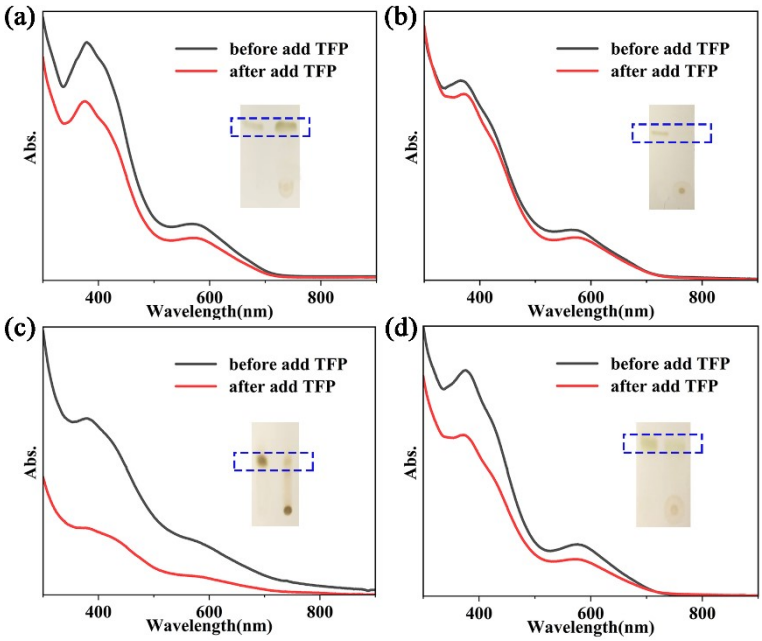

Fig. S1 UV changes of $Au_{36}(SR)_{24}$ before and after adding TFP (a) SR = 4-tert-butylbenaenethiol; (b) SR = 3-methylbenzenethiol; (c) SR = 4-methoxybenzenethiol; (d) SR = 2,5-dimethyl-benzenethiol ($Au_{36}(SR)_{24}$ are indicated with blue box).

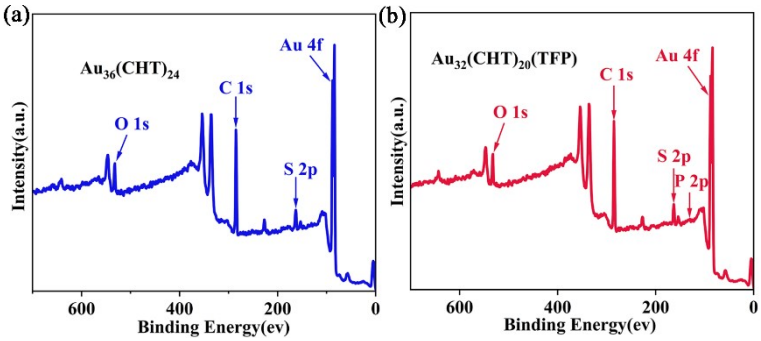

Fig. S2 XPS of (a) $Au_{32}(CHT)_{20}(TFP)$ and (b) $Au_{36}(CHT)_{24}$.

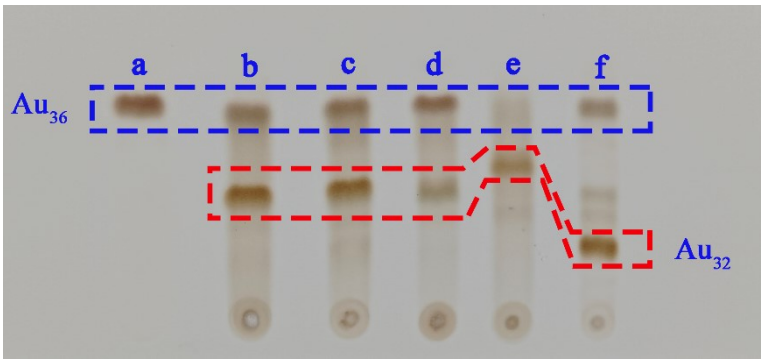

Fig. S3 Result of the reactions between $Au_{36}(CHT)_{24}$ and different monophosphine ligands. (a) No monophosphine; (b) tri(m-tolyl)phosphine; (c) tri(p-tolyl)phosphine; (d) tris(2-fluorophenyl)phosphane; (e) triphenylphosphine; (f) diphenyl-2-pyridylphosphine.

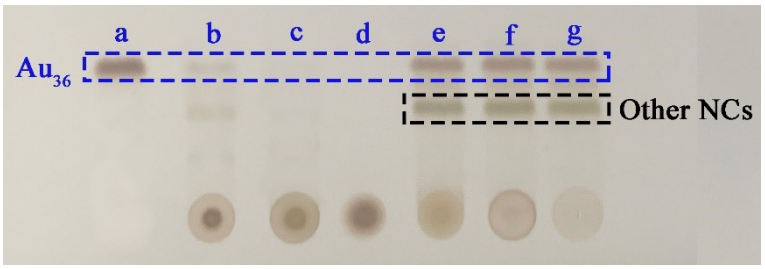

Fig. S4 Result of the reactions between $Au_{36}(CHT)_{24}$ and different diphosphine ligands. (a) No phosphine ligand; (b) 1,3-bis(diphenylphosphino)propane; (c) 1,2-bis(diphenylphosphino)ethane; (d) 1,1'-bis(diphenylphosphino)ferrocene; (e) bis(2-diphenylphosphinophenyl)ether; (f) racemic-2,2'-bis(diphenylphosphino)-1,1'-binaphthyl; (g) 4,5-bis(diphenylphosphino)-9,9-dimethylxanthene.

Table S2 Crystal data and structure refinement for $Au_{32}(CHT)_{20}(TFP)$.

CCDC	2424259
Empirical formula	$C_{133}H_{231}Au_{32}Cl_2O_3PS_{20}$
Formula weight	8924.16
Temperature/K	120.00
Crystal system	monoclinic
Space group	$P2_1/c$
a/Å	19.6005(6)
b/Å	31.8711(7)
c/Å	33.0905(11)
α/°	90
β/°	106.011(2)
γ/°	90
Volume/Å^3	19869.4(10)
Z	4
ρ_{calc}g/cm^3	2.983
μ/mm^{-1}	45.690
F(000)	15800.0
Crystal size/mm^3	0.4 × 0.2 × 0.05
Radiation	Cu Kα (λ = 1.54186)
2Θ range for data collection/°	8.206 to 104.998
Index ranges	$-13 \le h \le 20$, $-31 \le k \le 32$, $-34 \le l \le 21$
Reflections collected	58214
Independent reflections	21933 [R_{int} = 0.0774, R_{sigma} = 0.1130]
Data/restraints/parameters	21933/1673/1756
Goodness-of-fit on F^2	0.873
Final R indexes [I>=2σ (I)]	R_1 = 0.0616, wR_2 = 0.1471
Final R indexes [all data]	R_1 = 0.0958, wR_2 = 0.1558
Largest diff. peak/hole / e Å^{-3}	2.29/-1.98

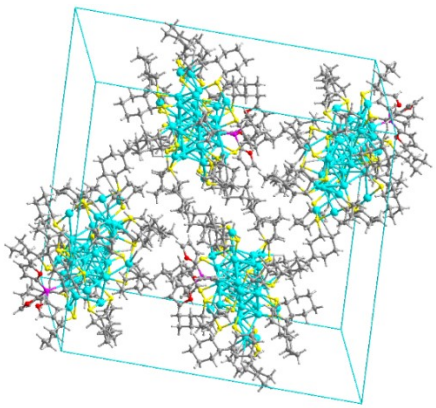

Fig. S5 A unit cell of crystal structure of $Au_{32}(CHT)_{20}(TFP)$. (Color coded: Au = blue; S = yellow; P = purple; O = red; C = gray; H = white).

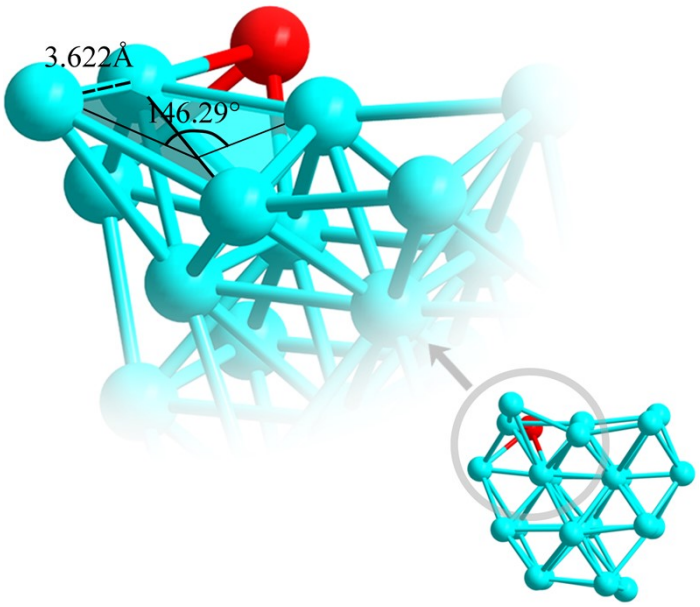

Fig. S6 Local amplification of Au_{24} kernel.

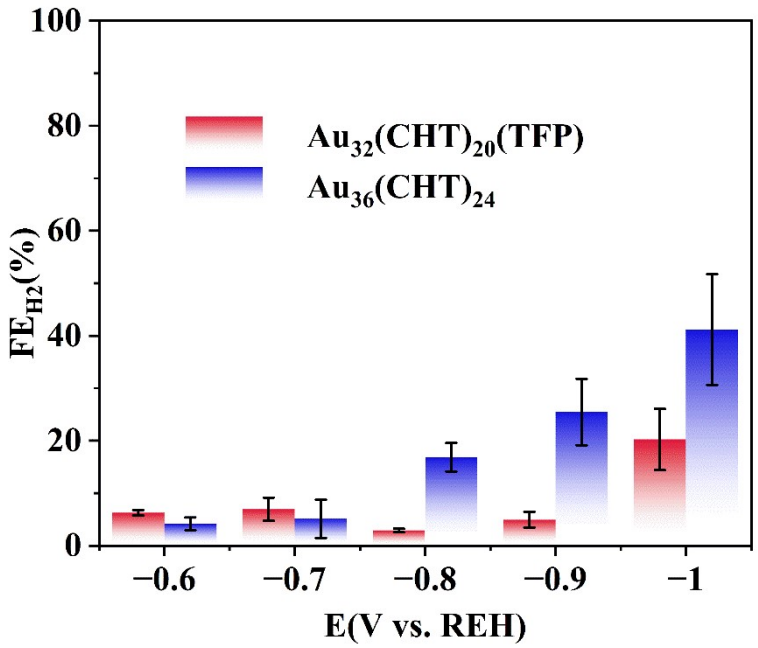

Fig. S7 H_2 Faraday efficiency of $Au_{32}(CHT)_{20}(TFP)$ and $Au_{36}(CHT)_{24}$ at different potentials.

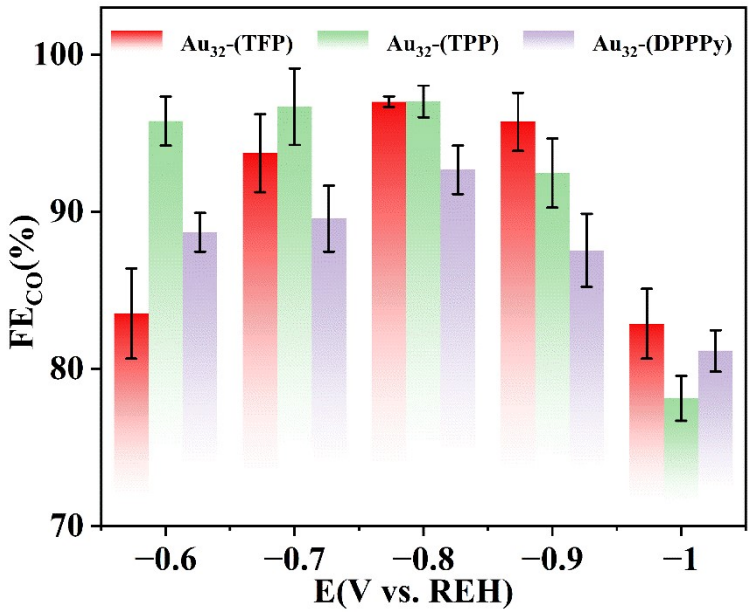

Fig. S8 The CO Faradaic efficiency for the Au_{32} containing different monophosphines as catalysts examined with different applied potentials.

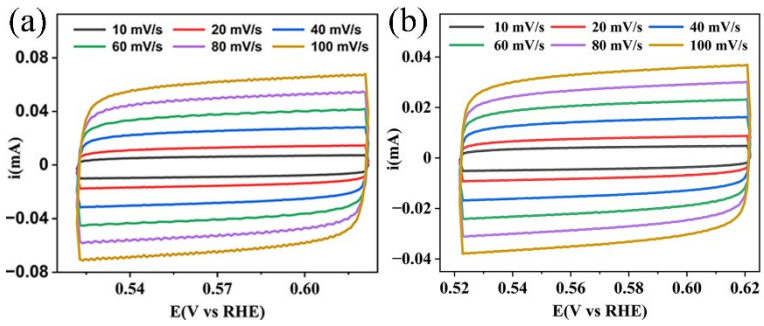

Fig. S9 The CV curves of (a) $Au_{32}(CHT)_{20}(TFP)$ and (b) $Au_{36}(CHT)_{24}$.

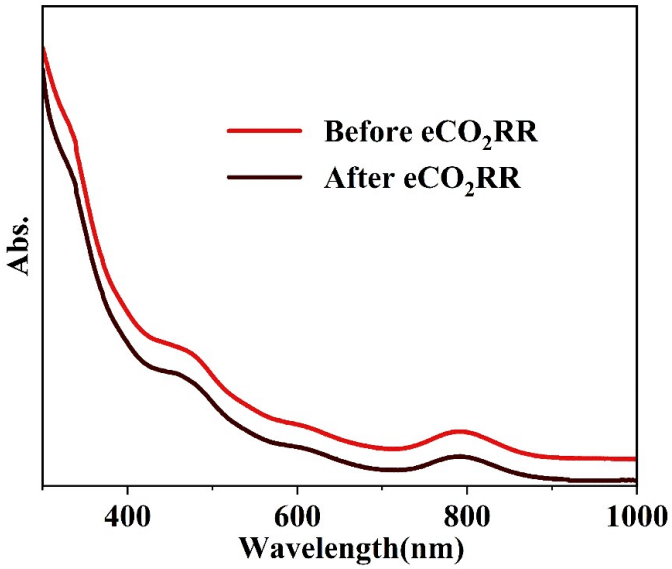

Fig. S10 UV-vis of $Au_{32}(CHT)_{20}(TFP)$ before and after performing eCO_2RR.

Table S3. FE_{CO} summary of partially summarized Cu nanoclusters.

Nanocluster	Highest FE/%
Au_{32}(This work)	97.7
Au_{36}	82.9
Cu_{17}[2]	91
Cu_8[3]	<10
Cu_6[4]	≈31.8
Cu_{26}[5]	≈80
Cu_{32}[6]	<5
Cu_{14}[7]	<10

References

1. P. R. Nimmala, S. Knoppe, V.R. Jupally, J. H. Delcamp, C. M. Aikens and A. Dass, $Au_{36}(SPh)_{24}$ nanomolecules: X-ray crystal structure, optical spectroscopy, electrochemistry, and theoretical analysis, J. Phys. Chem. B, 2014, 118, 14157-14167.
2. B. L. Han, L. C. Zhao, Z. R. Yuan, Z. Wang, Q. Yu, G. G. Luo, L. K. Wang, C. H. Tung and D. Sun, Dipropyne-Modified N-heterocyclic carbene stabilized atomically precise copper(I) nanocluster catalysts for CO_2 electroreduction, Adv. Funct. Mater., 2025, DOI 10.1002/adfm.202500149.
3. L. J. Liu, Z. Y. Wang, Z. Y. Wang, R. Wang, S. Q. Zang and T. C. W. Mak, Mediating CO_2 electroreduction activity and selectivity over atomically precise copper clusters, Angew. Chem. Int. Ed., 2022, 61, e202205626.
4. S. Li, X. Yan, J. Tang, D. Cao, X. Sun, G. Tian, X. Tang, H. Gou, Q. Wu, J. Sun, J. He and H. Shen, Cu_{26} nanoclusters with quintuple ligand shells for CO_2 electrocatalytic reduction, Chem. Mater., 2023, 35, 6123−6132.
5. Q. Tang, Y. Lee, D. Y. Li, W. Choi, C. W. Liu, D. Lee and D. e. Jiang, Lattice-hydride mechanism in electrocatalytic CO_2 reduction by structurally precise copper-hydride nanoclusters, J. Am. Chem. Soc., 2017, 139, 9728−9736.
6. Y. Shingyouchi, M. Ogami, S. Biswas, T. Tanaka, M. Kamiyama, K. Ikeda, S. Hossain, Y. Yoshigoe, D. J. Osborn, G. F. Metha, T. Kawawaki and Y. Negishi, Ligand-dependent intracluster interactionsin electrochemical CO_2 reduction using Cu_{14} nanoclusters, Small, 2024, DOI: 10.1002/smll.202409910.